Deformation and fragmentation behaviour of exploded metal cylinders and the effects of wall materials, configuration, explosive energy and initiated locations

Tetsuyuki Hiroe*, Kazuhito Fujiwara, Hidehiro Hata, Hirotsugu Takahashi
Department of Mechanical System Engineering, Kumamoto University, Kumamoto 860-8555, Japan

Abstract

Tubular metal specimens are explosively expanded to fragmentation, and the effects of wall materials, thicknesses, notches in walls, explosive driver diameters and the initiated locations are investigated on the deformation and fracture behavior of the cylinders experimentally and numerically. In the standard tests, the driver is a column of low density powder of high explosive PETN, inserted coaxially into the bore of a smooth-walled cylinder and initiated by exploding a bundle of fine copper wires at the column axis using a discharge current from a high-voltage capacitor bank. Notched cylinders with single axial slit, various grooves in the walls, and smooth cylinders with varied wall thicknesses were tested. Low-carbon steels and an aluminium alloy A5052 were provided in addition to the standard smooth-walled 304 stainless steel cylinder, and they were fully or partially charged with varying explosive column diameters. The initiated locations in the explosive column are changed for comparison, placing the bundle of fine copper wires eccentrically from the central axis or replacing the fine wire bundle into a bold wire line except the middle portion at the central axis for central point initiation. Additionally an explosive-filled cylindrical vessel with welded endplate at the one end is initiated at the other end explosive surface exploding wire-rows and expanded by axially propagating explosive detonation to fracture for comparison with the uniform expansion.

Deformation and crack initiation of expanding cylinders are observed with high speed camera, and most of the fragments have been recovered successfully. Recovered fragments have been measured and investigated using a fragmentation model. The effects of test parameters on the deformation and fracture behavior of metallic cylinders are discussed with use of numerical simulations, indicating applicability of the fragmentation model and suggesting future necessary studies.

Keywords: Fragmentation; Cylinder expansion; Explosive loading; Wire explosion technique

1. Introduction

Explosively loaded systems are the experimental techniques requiring the least capital investment,

* Corresponding author. Tel.: +81-96-342-3690; fax: +81-96-342-3729.
E-mail address: hiroe@gpo.kumamoto-u.ac.jp

and are suited [1] for start-up of a shock-loading research program. The authors have applied the wire-explosion techniques to develop such explosive loading devices [2-5] producing planar, imploding, and diverging detonation waves using powder pentaerythritol-tetranitrate (PETN). The generated cylindrically expanding detonation waves were used to examine the dynamic response of steel cylinders at high strain rates of 104 s-1 [4], which is one-order higher strain rate than those in similar studies [6]. Most of the fragmentation models [7] for cylinders are based on axially phased detonation initiated at one end of the cylinders.

In this study, rapid uniform expansion and fragmentation behavior for a fully explosive-charged smooth cylinder of 304 stainless steel are compared with those for the tests of cylinders with different parameters such as wall materials, amount of explosive charge, wall thicknesses, notches (groove or slit) and explosive-initiated locations. Most of the observed deformation behaviour are reproduced by the numerical simulation using Autodyn 2D. The effects of test parameters on fragmentation are investigated, suggesting future necessary studies [8] on mechanical changes in materials caused by precompression shock waves and a modification of the Grady model.

2. Experimental procedure

Experiments were performed utilizing the explosion test facilities at the Shock Wave and Condensed Matter Research Center, Kumamoto University. The developed test assembly for axially uniform or axially phased rapid expansion of cylinders driven by explosives is illustrated in Fig. 1(a), (b), (c) and (d). Fig. 1(a) shows a basic test assembly for tubular specimens of four kinds of metals: 304 stainless steel (304SS), A5052 and two kinds of carbon steels (C.S/ A and B) were explosively expanded to fragmentation. Table 1 shows the material properties used in this study. A column of the high explosive PETN (powder explosive made by Asahi Kasei Chemicals Ltd., charged density: 0.90-0.95 g/cc) was inserted into the central bore and initiated by exploding a bundle of three copper wires (diameter 175 μm) set along the central axis of the column using a discharge current from a high-voltage capacitor bank (40kV, 12.5 μF). The cylindrical diverging detonation wave and generated gas becomes the driver for the cylinder specimens. Specimens were machined from drawtubes to the cylinders of 100 mm length, outer diameter (D_o): 34-38 mm and wall (t): 3-3.5 mm as standard test specimens for every material. Mostly PETN columns filled the steel tubes, but, partially charged smaller diameter changes were also provided for cylinders of 304SS, A5052 and C. S. /A. In latter cases an air-layer between the explosive and the cylinder wall is left. In addition, explosive-filled cylindrical vessels with welded endplate at the one end are provided for 304SS and C.S/B and C, and initiated at the other end surface by exploding fine cooper wire rows as shown in Fig. 1 (b) and expand by axially propagating explosive detonation to fracture for comparison with the uniform expansion. Other type cylinders with varying wall thickness t: 1.65 mm, 6 mm (Do: 40 mm) and notched cylinders with single/double axial/circumferential grooves (GR; 1.5 mm width and depth on the inside/ outside wall surfaces) or single axial slit (SL; 1.5 mm width, space: filled with paste) in the walls were also provided as shown in Fig. 1(c) and compared with smooth wall cylinder (SM) for only 304SS cylinders. Additionally, the initiation location in the explosive column were changed and compared by placing the bundle of fine copper wires 7mm eccentrically from the central axis or replacing the fine wire bundle into a bold wire line except the middle portion (a fine wire line of 5mm length) at the central axis for central point initiation for 304SS cylinders as shown in Fig. 1(d). The dimensions of specimens and

explosives for four kinds of test types or groups are tabulated in Table 2. All the test conditions in this study are summarized as test No.1-22 in Table 1. At least two tests: observation of expansion behavior and recovery of fragments were conducted for every test condition, because both can not be completed at one test.

Deformation and crack initiation of expanding cylinders were observed with high speed cameras: IMACON 468 and Shimadzu/HPV-1 (frame rate of 30-10^6 fps), using a combination of lights from a xenon lamp as a back light and front lit by the use of mirrors to reflect the flash of exploding wires at the both edges of the cylinder. The fragments of exploded specimens were recovered for all the test conditions in a steel chamber filled with waste cloth.

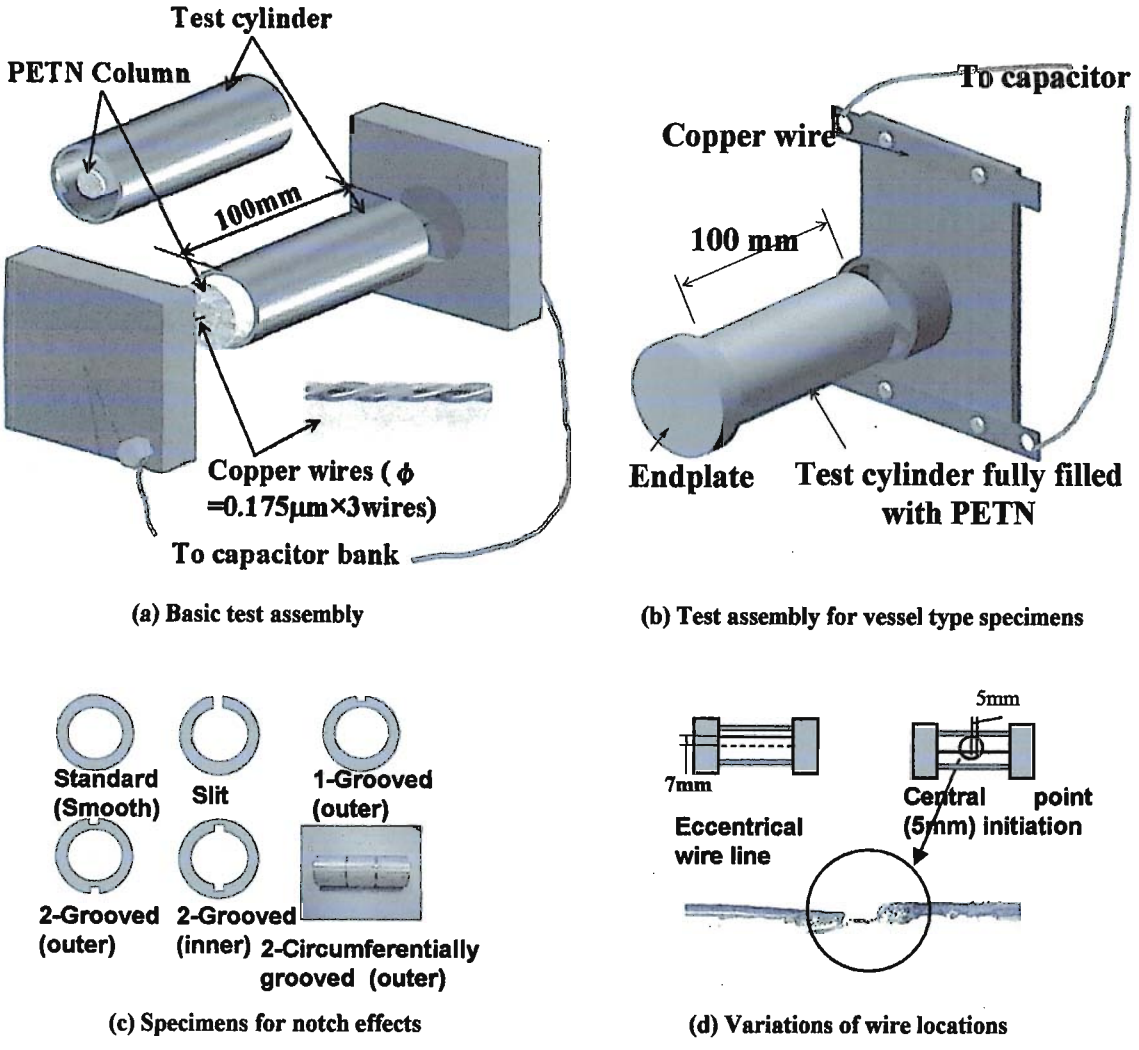

Fig. 1. Schematics of test assemblies for (a) uniform explosion of cylinders and (b) axially propagating expansion of vessels, (c) wall configurations for notch effects, and (d) varied wire-locations

Table 1. Material properties used in this study

Material symbol		304SS		A5052	C.S/A	C.S/B	C.S/C
Tube / plate		Tube	Plate	Tube	Tube	Tube	Plate
Material names and contents	JIS	SUS304		A5052TD-H34	SGP-E-G	STKM-13A	S55C
	contents	18%Cr-8%Ni stainless steel		2.5% Mg aluminium alloy	0.14% carbon steel	0.25% c. steel	0.55% c. steel
Tensile strength ,MPa		*(> 520)		274, (> 235)	—	435, (>370)	(>539)
Yield stress (0.2%proof stress), MPa		220, (>205)		264, (> 175)	190	420, (>215)	(>392)

* values inside parenthesis are those written in Japan Industrial Standard (JIS); others are those in mil-sheets

Table 2. Dimensions of test specimens and explosives for test types

Test Types	Mat.	Cylinder sizes, mm D_o	t	L	Size parameters, mm				
Wall thick	304SS,	34, 40	t	100	t = 1.65, 3, 6 (D_o=40)				
PETN diameter	304SS, C.S/A	34	3	100	PETN dia. = 28, 16, 12 (304SS), 28, 16 (C.S/A)				
	A5052	35	3	100	PETN dia. = 29, 16, 8				
Notch effects	304SS	34	3	100	Axial one slit 1.5width	Axial one groove(out) 1.5w x1.5d	Axial two groove(in) 1.5wx1.5d	Axial two groove(in) 1.5wx1.5d	Circumferential two groove(in) 1.5w x1.5depth
Initiation locations	304SS	34	3	100	1) Eccentric line (offset:7)		2) Central short line (5L)	3) Endsurface of PETNcolumn, (Vessel endplate: 50ϕ x 6t)	
	C.S/B	38	3.5	100	1) Central short line (5L)		2) Endsurface of PETN column, (Welded Vessel endplate: 48ϕ x 6t)		

3. Experimental and numerical expanding behaviour

Fig. 2 shows typical framing records for a fully charged smooth-walled standard cylinder of 304SS expanding symmetrically and uniformly. A number of crack initiation and axial propagation are seen on the surface at 16 and 22 μs, these features were also seen in other smooth-walled cylinders of A5052 and carbon steels A/B. Fig. 3 shows the comparison of streak camera records at the mid-length for exploding fully charged cylinders of 304SS with the different wall configurations: (a) smooth, (b) axially singly grooved and (c) axially singly slit walls. For grooved wall cylinder, early gas venting is seen at 20 μs only in the groove, and for slit wall cylinder, detonation gas starts venting at the instance of detonation arrival at the slit, but we see overall deformation behaviour is similar to that of the smooth wall cylinder. The values of $\dot{R}/R$: strain rates accurately only for uniform expansion of standard cylinders and wall velocities $\dot{R}$ at the estimated fracture initiation periods were 0.55-5.66× 10^4 s^{-1} and 130-1757 m/s for all the test conditions as listed in Table 3, where R is outer radius of the cylinder and the superscript dots denote differentiation with respect to time t. The $\dot{R}$ values are obtained from the average expansion rates at the periods from the streak camera records as shown in Fig. 3. Those values are smaller (60-90%) than Gurney velocities [9] as shown in Table 3. Fig. 4 shows typical framing records for exploding fully charged 304SS cylinders with smooth walls but anomaly initiated (a) with

an axial copper wire line placed eccentrically from the central line and (b) at a central point.

Table 3. Summary of experimental conditions and observed deformation data

No	Mat.	Initiation locations	Cylinder types /Vessel	Cylinder sizes, mm			PETN dia, mm	$^{*}\dot{R}$, m/s	Gurney vel., m/s	$^{*}\dot{R}/R$, $(\dot{\varepsilon})$, $10^{4}s^{-1}$
				D_o	t	L				
1	304SS	C. Axis	Smooth(standard)	34	3	100	28/full	1000	1154	3.66
2	304SS	C. Axis	Smooth(standard)	34	3	100	16	348		1.33
3	304SS	C. Axis	Smooth(standard)	34	3	100	12	130		0.55
4	304SS	C. Axis	Smooth	34	1.65	100	30.7/full	1367	1564	4.97
5	304SS	C. Axis	Smooth	40	6	100	28/full	450	761	2.00
6	304SS	C. Axis	A.1 Slit	34	3	100	28/full	1000		3.66
7	304SS	C. Axis	A.1 Slit	34	3	100	16	398		1.57
8	304SS	C. Axis	A.1 Grooved	34	3	100	28/full	983		3.82
9	304SS	C. Axis	A. 1Grooved	34	3	100	16	382		1.51
10	304SS	C. Axis	A. 2Grooved	34	3	100	28/full	1000		3.76
11	304SS	C. Axis	A. 2Grooved (in)	34	3	100	28/full	900		3.44
12	304SS	C. Axis	C. 2Grooved (in)	34	3	100	28/full	1184		4.52
13	A5052	C. Axis	Smooth(standard)	35	3	100	29/full	1757		5.66
14	A5052	C. Axis	Smooth(standard)	35	3	100	16	915		3.28
15	A5052	C. Axis	Smooth(standard)	35	3	100	8	280		1.26
16	C.S./A	C. Axis	Smooth(standard)	34	3	100	28/full	1180		3.75
17	C.S./A	C. Axis	Smooth(standard)	34	3	100	16	417		1.50
18	C.S./B	C. Axis	Smooth(standard)	38	3.5	100	31/full	863		3.12
19	304SS	Ecc. Axis	Smooth(standard)	34	3	100	28/full	968	1145	3.06
20	304SS	C. Point	Smooth(standard)	34	3	100	28/full	1275	1127	4.97
21	304SS	End-surface	Vessel	34	3	100	28/full	1073		3.73
22	C.S./B	End-surface	Vessel	38	3.5	100	31/full	1043		2.53

$^{*}\dot{R}$, $\dot{R}/R$, $(\dot{\varepsilon})$ are the data at the estimated fracture initiation period, and derived from an average expansion rate at the central portion of cylinder.

Wire-explosion (3μs) Expansion (9μs) Crack growth (16μs) Fragmentation (22μs)

Fig. 2. Typical framing records for an exploding standard 304SS cylinder with fully charged PETN (test No. 1)

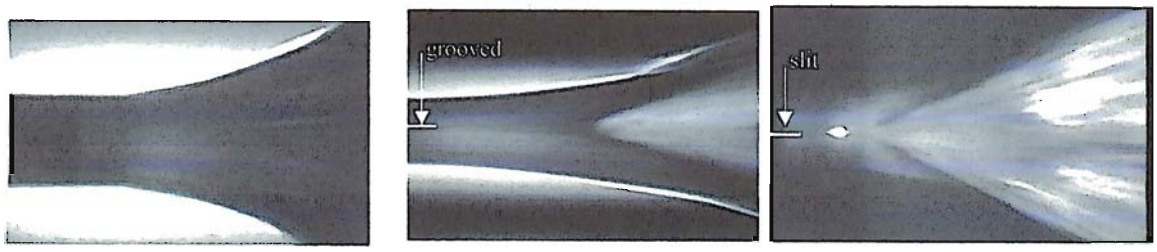

(a) Smooth (test No. 1) (b) Groove (Grooved on front side, test No. 8) (c) Slit (Slit on front side, test No. 6)

Fig. 3. Streak records at the mid-length for exploding fully charged cylinders of 304SS with (a) smooth, (b) one-grooved and (c) slit walls – test No. 1, 8 and 6 respectively.

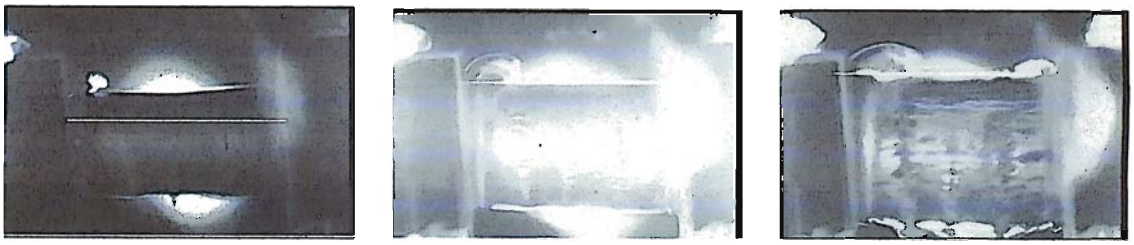

(a) Initiated at an eccentrically placed axial line; see an inserted white line on the first photo (test No.19)

(b) Initiated at a central point (a short line of 5mm), see a white mark laid on the first photo (test No. 20)

Fig. 4. Typical framing records for exploding fully charged standard 304SS cylinders with smooth walls anomaly initiated (a) at an eccentrically placed axial line and (b) a central point - test No. 19 and 20 respectively

A white line and a white mark inserted on the first photos represent the initiated line and point respectively. In case of eccentric line initiation, axially uniform expansion behaviour is similar to that of the standard cylinder except a considerable time gap in deformation start at the top and bottom sides of the cylinder. Circumferential corrugations during expansion were often seen in other test cases and it seems to be a local expansion caused by reduction of area due to the axial tensile stress. In the latter

case of central initiation, wall velocity at the mid-length of the cylinder is 28% larger than that in the uniform cylinder expansion as shown in Fig. 3(a) and summarized at Table 3. The streak and framing records for the axially phased expanding casing model vessels showed the radial wall velocities were slightly larger than those of the corresponding uniformly expanded cylinders, and the initial fracture occurred at the welded joints of a cylinder and an end plate.

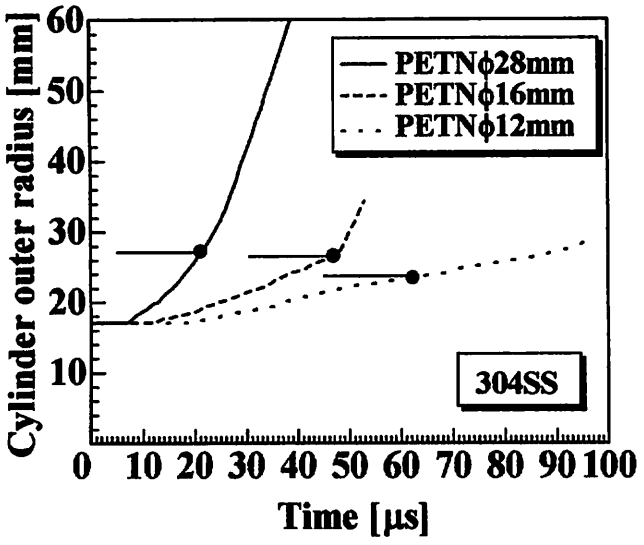

(a) 304SS smooth cylinders with PETN variations (test No. 1, 2 and 3)

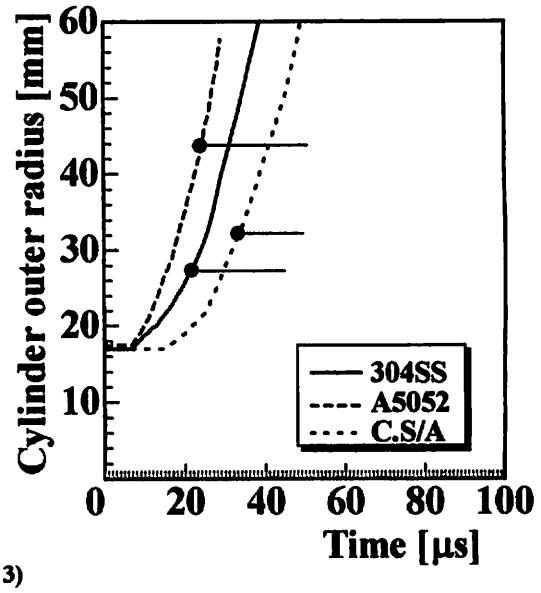

(b) Fully charged cylinders of three materials (test No. 1, 13 and 16)

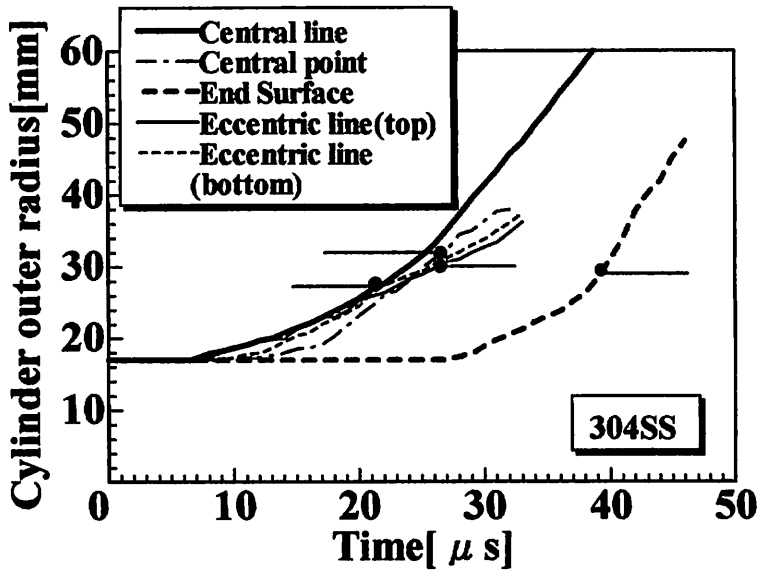

(c) Fully charged cylinders and a vessel of 304SS, showing the effects of the initiation locations (test No. 1, 19, 20, 21)

Fig. 5. Experimental time-histories of wall radii at the mid-length for expanding (a) smooth cylinders with variations of charged PETN diameters and wall materials, and (b) 304SS smooth cylinders with variations of initiated locations; standard central line, eccentric axial line (top: near wall, bottom: far wall), central point and end-surface (vessel). Horizontal lines and dots show the fracture radii estimated from the thicknesses of recovered fragments. See corresponding test numbers in Table 3.

Time-histories of expanding outer wall radii at the mid-length of the cylinders obtained from the streak records are shown in Fig. 5 for expanding (a) smooth cylinders with variations of charged PETN diameters and (b) wall materials, and (c) fully charged 304SS smooth cylinders with variations of initiated locations; standard central line, eccentric axial line (top: near wall, bottom: far wall), central point and end-surface (vessel). Horizontal short lines in the figure show the fracture radii R_f estimated from the thicknesses of recovered fragments. Fig. 5(b) represents that fully explosive-charged cylinders expand earlier in ascending order of A5052, 304SS and carbon steel/ A, but the average expansion velocities are very similar for 304SS and C. S. /A except in the final stages of acceleration for 304SS. These phenomena seem to be related with dynamic stress-strain relations of materials and lower yield stress and larger work-hardening of 304SS compared with carbon steel. The explosive energy or PETN column diameter effect on cylinder expansion is also predicted. Fig. 5(c) represents overall time-histories of wall radii for the cylinders with variations of initiated locations. The time-histories are almost similar to that of uniformly expanding standard cylinder, and only the cylinder initiated at the central point expands a little faster at the mid-length. Such deformation phenomena resemble the observed insensitivity to notches inserted in cylinders, and these seem to be characteristics for rapid expansion of cylinders with the expansion rate of over 10^4 s^{-1} as shown in this study.

Numerical simulations were performed for all the experiments using a hydro code, Autodyn 2D based on finite difference method (FDM) and smoothed particle hydrodynamics (SPH), examining the experimental expanding behaviour, numerical stresses and fracture criteria of the cylinders, where the Johnson-Cook constitutive model [10] (A5083H116 for A5052 and steel 1006 for carbon steels) and the Steinberg model [11] (304SS) are adopted. Experimental and numerical time-history curves of outer wall radii of cylinders coincided well for most cases, and the disjunction of both curves or fracture radii suggests a critical fracture strain of ε_f (=ln($2R_f/D_o$)). Fig. 6 (a), (b) represents typical examples of numerical simulations. The former example (a) shows numerical time-histories of circumferential stresses in the wall at the mid-length for a fully charged standard cylinder of 304SS. It is seen that prior strong compressive pulses are present before the following tensile stresses grow, and the period when all the stresses in the wall reach the equal value of 1.2 GPa corresponds with the estimated fracture time shown in Fig. 6. Such cyclic large precompressive stress waves must have changed the mechanical properties and affected the following fracture of the cylinders. Preliminary tests [8] produced the results which support this assumption using momentum trap technique. The latter example (b) shows the numerical pressure distributions at 23.5 μ s for casing model vessel of 304SS just after the spallation has been generated, indicating negative pressure distribution and the occurrence of spallation (used critical stress value: 1.0GPa) in the endplate numerically. This numerical overall deformation and spallation have reproduced the observed results well.

4. Fragmentation and discussions

In the investigation on fragmentation, fragment recovery tests were performed and most fragments (81-96%) were successfully recovered for all the test conditions inside a cushion-filled chamber without secondary damage. 61% was collected for the cylinder with the thinnest wall. Fig. 8 (a), (b) and (c), (d) show typical recovered fragment photos for 304SS cylinders and the comparison of those for smooth wall cylinders with different initial wall thickness of 1.65, 6 mm and slit wall cylinders (3mm thickness) with different explosive charges.

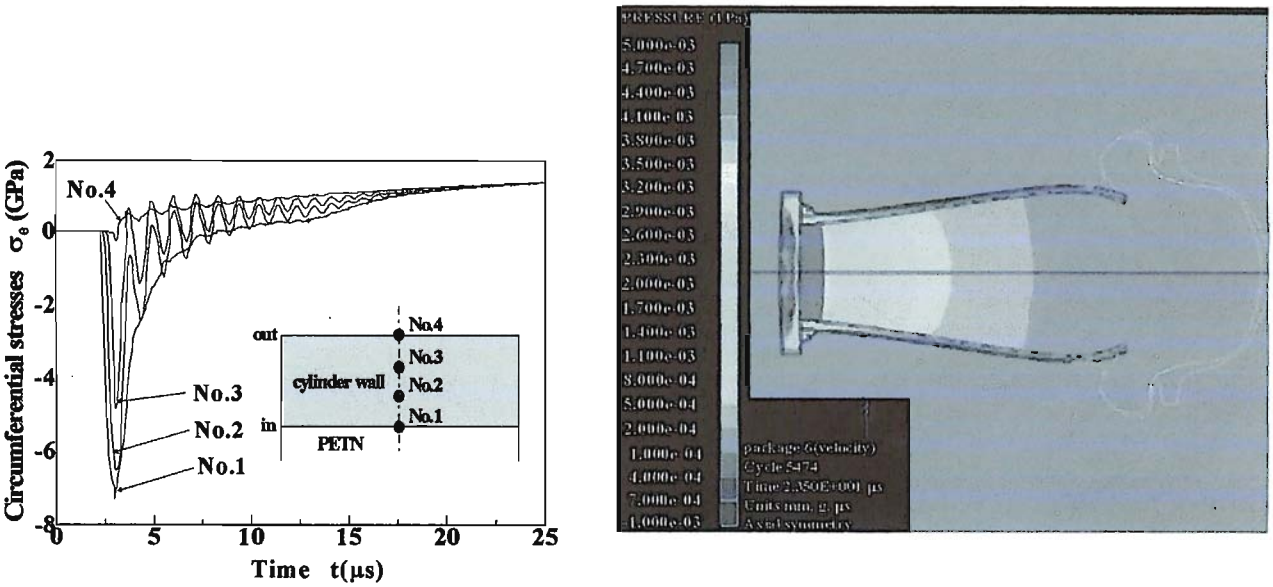

Fig. 6. Typical examples of numerical simulations: (a) time-histories of circumferential stresses (minus stress value means compression) in the wall at the mid-length for a standard cylinder of 304SS with fully charged PETN and (b) pressure distributions at 23.5 μs for casing model vessel of 304SS, showing the situation just after the spallation has been generated numerically in the endplate.(Large compression and tension are expressed similar for grey scale.)

The fragments in the photos are placed from large to small ones except those of edge and notched part of the cylinder which are easily discriminated examining the machined surface of the fragments. It is generally seen that fracture of the cylinder portion is predominantly along elongated strips, with the fracture parallel to the axis. Most of the fragments are 3-6 times longer than they are wide, and shear fracture appears to be the dominant mechanism for all the materials. In measurement of average widths of fragments used for fragmentation energy later, a modification procedure was adopted because the applied fragmentation model [7] for cylinders is one-dimensional, that is, the widths of longer fragments have larger count numbers than shorter ones and vice versa. The thinly walled or fully charged cylinders expand more rapidly, and their fragments apparently become smaller or narrower than those of thick walled or smaller charged ones as shown in figures (a)/(b) and (c)/(d). This basically matches the fragmentation model mentioned later. The comparison of recovered fragments has indicated that the fragments of fully charged notched wall cylinder (slit or grooved) are almost similar to those of the smooth wall cylinder except those neighbouring on the notch (groove or slit) which are notably larger than others (see Fig. 9 (a) later), but in cases of partially charged explosive or lower expansion velocity, strain-rate effects on fragment sizes of notched cylinders becomes remarkable suggesting the notches as an additional parameter in fragmentation as shown in figure (c), (d). The fragment thicknesses lead to the critical strains based on the volume constant hypothesis, and the values correspond with those estimated so far from streak records.

In this study, the Grady's fragmentation energy Γ $(=\rho\dot{\varepsilon}\, S^3/24)$ [7] where ρ ; the density of materials,

S: circumferential width of fragments and $\dot{\varepsilon}(=\dot{R}/R)$: circumferential strain rate at estimated fracture time was obtained for all the test cases.

Figure 9 shows typical histograms of Γ values of 304SS fragments for (a): fully charged smooth and notched cylinders, (b): partially charged smooth and notched cylinders, (c): fully charged smooth cylinders with various wall thicknesses and (d): fully charged cylinders with various initiated locations. If the model is perfect, the average values of Γ for smooth walled cylinders should remain within a narrow range as a material constant in all the test cases except thinnest cylinder (t: 1.65mm), see Fig.9 (c) where the secondary deformation of thin fragments reduced accuracy in measurement, but actually it was revealed that the Γ values based on the model varied depending on the strain rates or driving explosive energy. The notch effects on Γ values were negligibly small for fully charged cylinders in Fig. 9 (a) but become noticeable in case of partially charged or slowly expanded cylinders as shown in Fig. 9 (b) and already mentioned Fig. 8 (c) (d), suggesting need of a modification factor α for the notch effect in the model: $\Gamma = \alpha\rho\dot{\varepsilon}\, S^3/24$. Further study is necessary to extend the applicability of this equation to all the types of notches. Such strain-rate dependency was seen on the Γ values for smooth cylinders of A5052 and carbon steels. Fig. 9 (d) shows that the effects of initiated locations are small for axially phased expansion tests but rather considerable for eccentric line initiation tests and central point initiation tests.

The measured average data of fragment sizes: width S and thickness h and calculated Γ values based on Grady's model are summarized for all the test cases as shown in Table 2, where test numbers

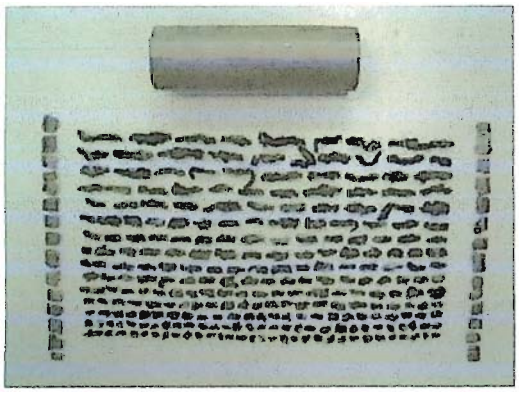

(a) Smooth thin walled cylinder: t=1.65 mm (PETN filled up) – Test No. 4

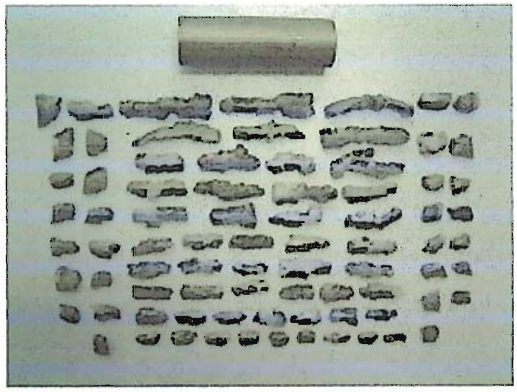

(b) Smooth thick walled cylinder: t=6 mm (PETN filled up) – Test No. 5

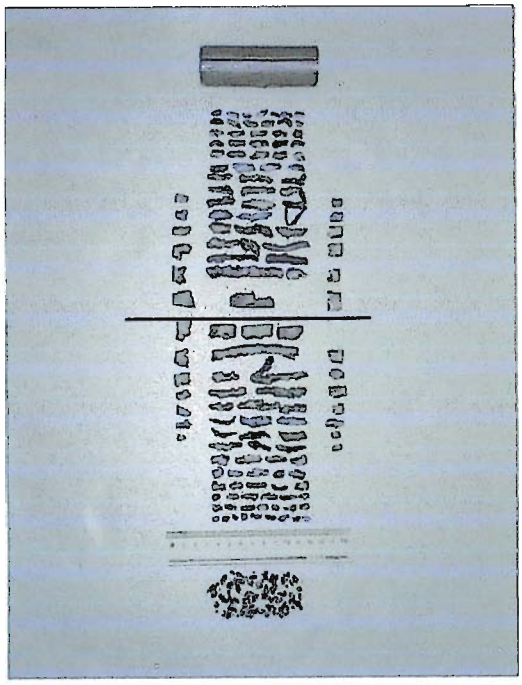

(c) Slit cylinder, PETN filled up: ϕ=28mm (wall thickness: 3mm) – Test No. 6

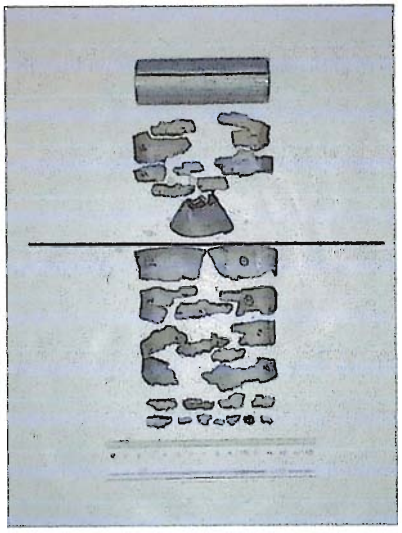

(d) Slit cylinder, PETN partially filled: ϕ=16mm (wall thickness: 3mm) – Test No. 7

Fig. 7. Typical photos of recovered fragments of uniformly exploded cylinders of 304SS (a): Smooth cylinder with thin wall (fully charged), (b): Smooth cylinder with thick wall (fully charged), (c): Slit cylinder (PETN fully charged), (d): Slit cylinder (PETN partially charged). Sold lines show the location of slits.

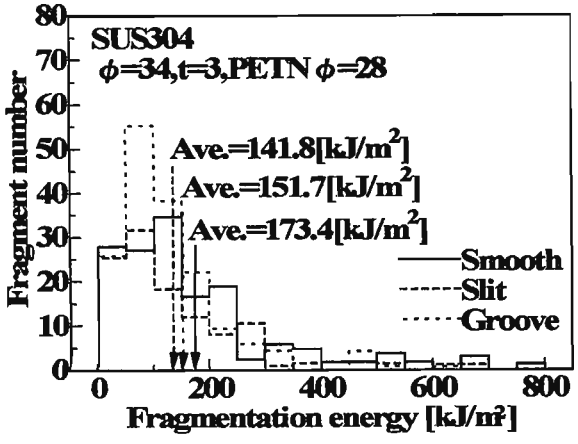

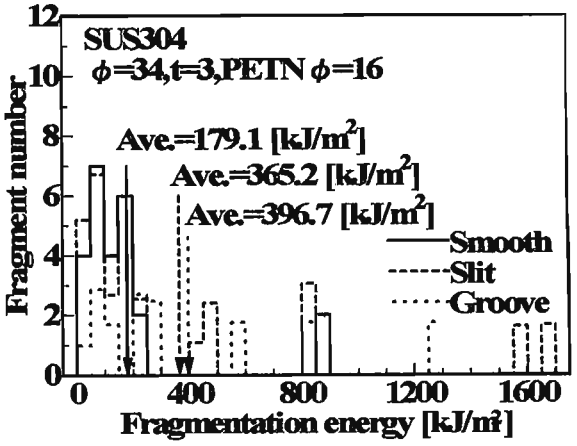

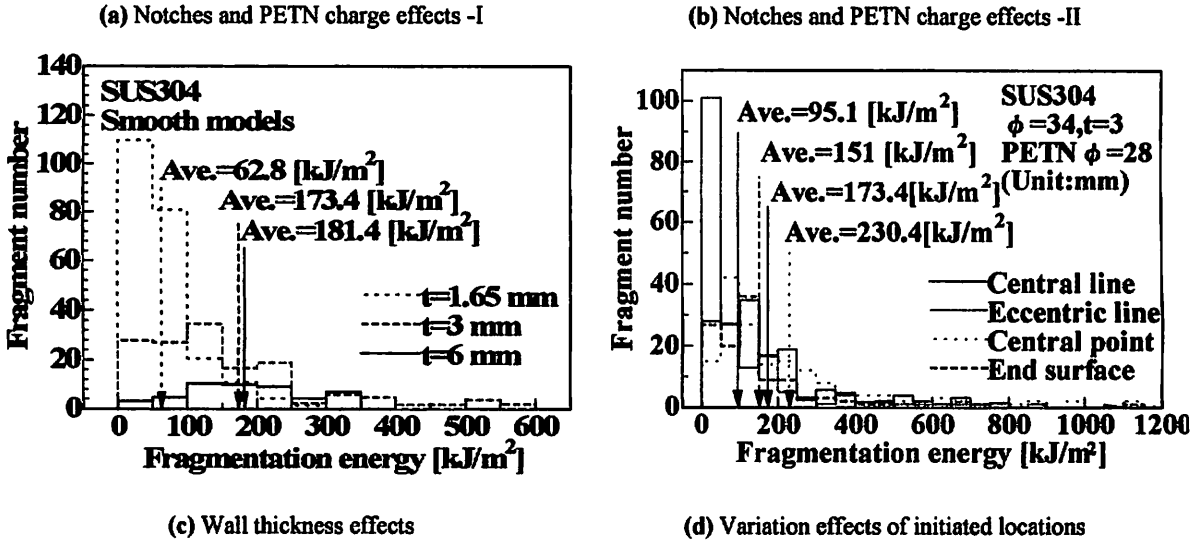

Fig. 8. Typical histograms of fragmentation energy for 304SS based on Grady's model for (a): fully charged smooth & notched cylinders, (b): partially charged smooth & notched cylinders, (c): fully charged smooth cylinders with various wall thicknesses and (d): fully charged cylinders with various initiated locations

correspond with those in Table 1. Fig. 10 expresses the relations between Γ values and strain rates of cylinder walls for all the test cases, showing four data groups: 304SS (smooth), 304SS (notched), A5052 and C. S. (A, B). It is known that Γ values are not constant for materials and decrease as the strain rates increase for A5052 and carbon steels A/B and vice versa for 304SS. The authors have a bold assumption that the phenomena are related with mechanical changes [12] in materials caused by precompression shock waves as shown in Fig. 7 (a), although cylinder fragmentation phenomenon must involve experimental errors and uncertainty. Authors' other study [8] on mechanical changes by pre-shockwaves indicates growth of yield stress and reduction of fracture ductility ε_f for both an aluminium alloy and 304SS, and their product may be closely related with fragmentation energy of materials and the degrees of mechanical changes differ in materials showing similar features for their products to the results in this study.

Table 4. Summary of measured average data for fragment sizes: width S, thickness h and calculated fragmentation energy values Γ based on Grady's model

No		1	2	3	**4	5	6	7	8	9	10
Fragment	h	1.76	1.84	2.05	0.99	5.12	1.72	1.91	1.86	1.91	1.81
sizes, mm	S	6.78	13.1	19.2	**3.83	10.7	6.26	14.1	6.31	15.5	7.70
Frag.Energy, Γ kJ/m²		173.4	179.1	94.2	**57.3	178.1	134.7	365.2	151.7	396.7	272.0

No	11	12	13	14	15	16	17	18	19	20	21	22
h	1.84	1.84	1.59	1.78	2.26	1.39	1.50	2.27	1.51	1.61	1.66	1.49
S	7.40	6.02	4.48	8.64	18.8	6.94	10.2	7.88	6.29	6.21	6.06	9.09
Γ	224.9	179.5	45.0	74.6	120.4	177.0	420.0	168.1	95.1	230.4	151	222.8

.**Very thin fragments folded at both sides

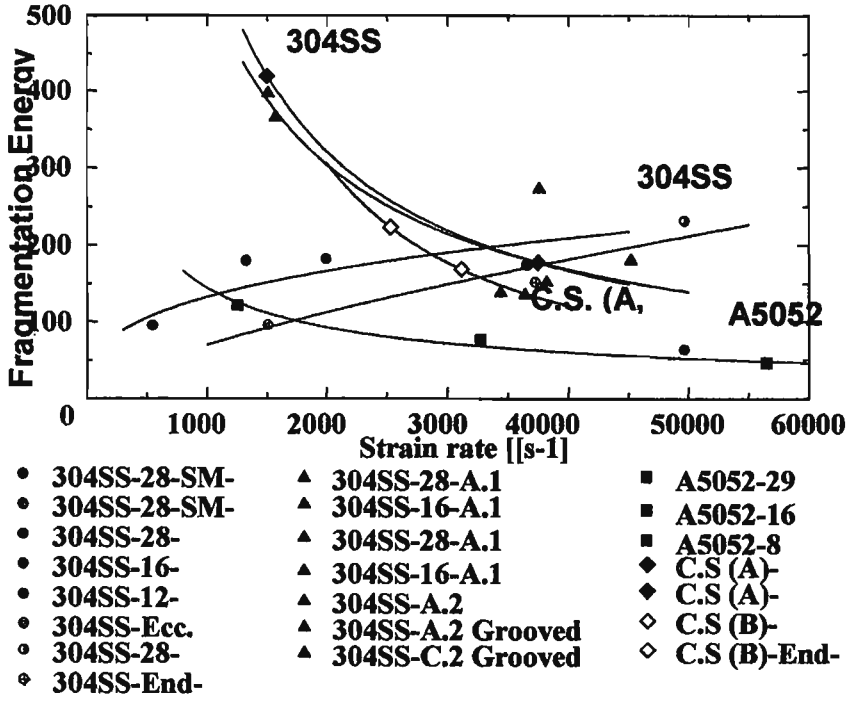

Fig. 9. Relations between fragmentation energy values calculated from Grady's model and strain rates for cylinders of 304SS(smooth) including variation of initiation locations, 304SS(notched), carbon steels C. S. (A, B) and A5052.

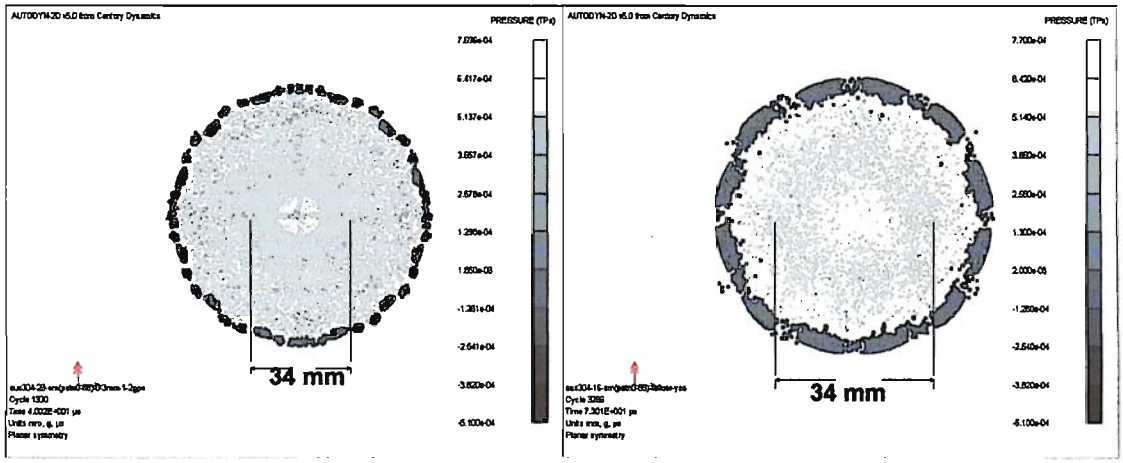

(a) (b)

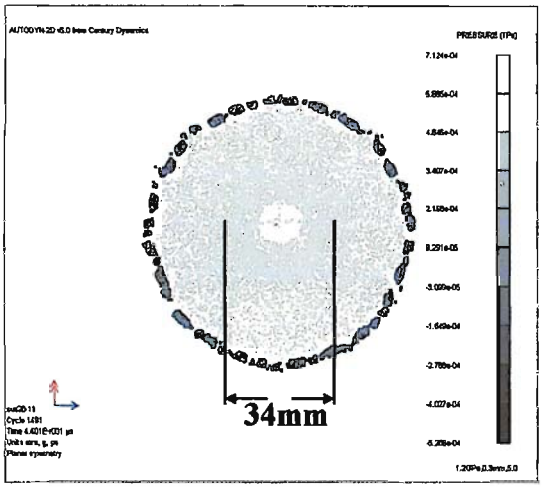

(c)

Fig. 10. Numerical fragmentation examples using a smoothed particle hydrodynamics processor and Mott's stochastic failure modeling in Autodyn2D for smooth 304SS cylinders with (a) fully charged (ϕ:28mm) PETN at 40μs, (b) partially charged (ϕ:16mm) PETN at 72μs and (c) fully charged and an eccentric initiation line (eccentric distance: 7mm to the top side) at 44μs. Average widths are 4.80, 8.63 and 4.32 mm for (a), (b) and (c).

Generally a stochastic failure model has to be introduced to impose some material heterogeneity or inherent microscopic flaws. In this study an investigation on numerical fragmentation is demonstrated using the SPH and Mott's stochastic failure model installed in Autodyn 2D: failure probability $P = 1 - \exp(-Ce^{\gamma\sigma}/\gamma)$, σ:1.2GPa, γ:16. Fig. 11 shows typical examples for smooth cylinders of 304SS with (a) fully charged (ϕ:28mm) PETN at 40μs, (b) partially charged (ϕ:16mm) PETN at 72μs and fully charged and (c) an eccentric initiation line at 44μs. There still exist some discrepancies between numerical and experimental average fragment widths but such numerical fragmentation tendency coincides with experimental results as shown in Fig. 8 (c), (d) and Table 2.

5. Conclusions

Tubular metal specimens are explosively expanded to fragmentation in 22 test conditions with various parameters: wall materials, thicknesses, notches, explosive driver diameters and the initiated locations at average strain rates or $\dot{R}/R$ values of $0.55\text{-}5.66\times10^4$ s^{-1} and a wall velocity of 130-1757 m/s. Observed and numerical cylinder expansion behavior indicated that the effects of explosive energy and wall materials on cylinder expansion are almost predictably but variations of initiated locations and notches in cylinder walls are rather insensitive to deformation behavior and such phenomena seem to be characteristics for rapid expansion of cylinders. The investigation on recovered fragments revealed that *the thinly* walled or plenty charged cylinder expands more rapidly, and its fragments apparently become smaller or narrower than those of thick walled or poorly charged one, which basically matches the Grady's fragmentation model, and notch effects on fragmentation are small at high strain rates but become noticeable at lower strain rates suggesting a modification factor for the model. The variations

of initiation locations affect not much but considerably, because overall expansion rates are essential and differ a little in this study. The experimental average fragmentation energy values based on the fragmentation model are not constant but differ depending on the strain-rates for every material of smooth cylinders and it seems related with mechanical changes in materials caused by explosive precompression shock waves. Some demonstrative numerical results have shown a possibility of simulation for fragmentation using the SPH processor and a stochastic failure model, as reported in past journals. In this paper, experimental acquisition of rapid expansion and fracture behavior of various types of cylinders is emphasized, and only 2-D analysis was applied to support the understanding of the phenomena, leaving 3-D detailed analysis for future study.

References

[1] Meyer MA. Dynamic behavior of materials. John Wiley & Sons, Inc., 1994.
[2] Hiroe T, Matsuo H, Fujiwara K, et al. A study on generation of plane detonation and strong imploding shocks by wire-row explosion. J. of the Japan Explosive Society 1996;57(2):49-54.
[3] Abe T, Yoshida M, Hiroe T, Fujiwara K, Matsuo H. Explosive-driven cylindrical imploding shocks in solid initiated with an exploded etched copper mesh. In: Proceedings of International Conference AIRAPT-16 and HPCJ-38 on High Pressure Science and Technology, Kyoto, Japan, 1998. p. 912-4.
[4] Hiroe T, Matsuo H, Fujiwara K, et al. Spall in metals induced by explosive shock loadings and protective measures using momentum traps. Trans. Japan Society of Mechanical Engineers A 1996; 62:2026-31.
[5] Hiroe T, Matsuo H, Fujiwara K, Abe T, Kusumegi K. Uniform expansion of cylinders at high strain rates using an explosive loading. In: Proceedings of International Conference on Condensed Matter under High Pressures, National Institute of Science Communication, New Delhi, 1998. p. 458-65.
[6] Forrestal MJ, Duggin BW, Butler RI. An explosive loading technique for the uniform expansion of 304 stainless steel cylinders at high strain rates. Trans ASME J of Applied Mechanics 1980;47:17-20.
[7] Grady DE, Hightower MM. Natural fragmentation of expanding cylinders. In: Proceedings of Shock-wave and High-Strain–Rate Phenomena in Material, Marcel Dekker, Inc., 1992, p.713-21.
[8] Hiroe T, Fujiwara K, Hata H, Watanabe K, Yamamoto M. Mechanical changes in materials caused by explosive precompression shock waves and the effects on fragmentation of exploding cylinders. In: Proceedings of 2nd International Symposium on Explosion, Shock Wave and Hypervelocity Phenomena, Kumamoto, Japan, 2007. (In print)
[9] Gurney R. The initial velocities of fragments from bombs shells and grenades. Report No. 405, Ballistic Research Laboratory, 1943.
[10] Johnson GR, Cook WH. A constitutive model and data for metals subjected to large strains, high strain rates, temperatures and pressures. In: Proceedings of the 7th International Symposium on Ballistics, Hague, Netherlands, 1983. p. 541-7.
[11] Steinberg DJ, Cochran SG, Guinan MW. A constitutive model for metals applicable at high-strain rate. J. Appl. Phys 1980;51:1498-504.
[12] Grady DE. The spall strength of condensed matter. J. Mech. Phys. Solids 1988;36(3):353-84.